



Optimization of micromixer with triangular baffles for chemical process in millidevices

Harrison S. Santana^{a,*}, João L. Silva Jr^b, Osvaldir P. Taranto^a

^a School of Chemical Engineering, University of Campinas, 13083-852, Campinas, SP, Brazil

^b Federal Institute of Education, Science and Technology of South of Minas Gerais – IFSULDEMINAS, 37560-260, Pouso Alegre, MG, Brazil



ARTICLE INFO

Keywords:

Micromixers
Baffles
Circular obstructions
Millidevices
Numerical simulation
Process intensification

ABSTRACT

A new micromixer design (MTB – micromixer with triangular baffles and circular obstructions) was proposed aiming the combination of three mass transfer enhancements mechanisms: reduction of molecular diffusion path, split and recombination of streams and vortex generation. The geometric variables were also optimized considering the mixing performance and the required pressure drop. The optimal design was used for the mixing of different binary mixtures (vegetable oil/ethanol and water/ethanol) under the Reynolds number range from 0.01 to 200 and the chemical reaction process of vegetable oil transesterification with ethanolic solution of sodium hydroxide (biodiesel synthesis). High mixing index ($M = 0.99$) was observed for the oil/ethanol mixing for several channel heights (200 μm – 2000 μm) and widths (1500 μm – 3000 μm). The geometry W3000H400 (i.e., MTB with channel width of 3000 μm and height of 400 μm) was employed as the millireactor, providing a maximum oil conversion of 92.67% for a residence time of 30 s. For the water/ethanol mixing, the geometry W1500H200 was used. High mixing index ($M = 0.99$) was observed at very low Reynolds number ($Re = 0.1$) and also in higher Reynolds numbers of 50 and 100. Moreover, at $Re = 0.1$, high mixing index ($M \geq 0.90$) was obtained already at 3.5 mm of channel length. However, for higher Reynolds number the fluids required longer distances to achieve superior mixing, about 10.5 mm at $Re = 100$. The MTB, unlike the ones found in the literature, can be used in microdevices (e.g., sensors) with low flow rates and in microdevices with large dimensions (eg, millidevices and milireactors) with high flow rates, allowing an easier application in chemical process aiming the commercial production.

1. Introduction

Process Intensification is a strategy for chemical plant size reduction achieving a determined production goal. In 1995, Ramshaw [1] stated the process intensification as the volume reduction in orders of 100 or more, assessed by the individual part size reduction or by the decrease of involved units. By the time, this level of volume reduction was very arduous to achieve. Therefrom, a promising technology in the field of system miniaturization, organic synthesis and energy production emerged and has been providing satisfactory results in the process intensification. This technology is known as Microfluidics, defined the Microfluidics as the science and technology that studies the fluid behavior and controlled manipulation and the design of device and systems capable to execute reliably tasks in microchannels of typical sizes about tens to hundreds of micrometers [2]. The Microfluidics tools allow obtaining great advantages in the microscale processes regarding the macroscale methods: low amount of reagents and samples, short

reaction times, low manufacturing costs, high surface area-to-volume ratio (about 20,000 $\text{m}^2 \text{m}^{-3}$ against 1000 $\text{m}^2 \text{m}^{-3}$ of conventional reactors) and high heat and mass transfer rates [3,4]. The application of microdevices includes biological systems, microsensors, microreactors and micro-heat exchangers [5–8].

The literature has been demonstrating some difficulties in the microdevices scale-up to the required processing volumes without missing the microscale transport phenomena characteristics. Researches in academia and industry have revealed additional efforts to approach the microdevices enlargement [9]. As example, taking the capacity of a biodiesel plant with a capacity of 2000 L day⁻¹ [10], 3.4×10^6 microreactor units operating under a flow rate of 5.8×10^{-4} L min⁻¹ would be required [7]. The high number of microdevices required is due to the micrometric dimensions, resulting in low flow rates. Fortunately, some researches on scale-up have exposed some interesting strategies for production rate increment using microdevices with larger sizes. These strategies include the scale-out by suitable dimension

* Corresponding author.

E-mail address: harrison.santana@gmail.com (H.S. Santana).

Nomenclature	
C	molar concentration (mol m^{-3})
d_H	hydraulic diameter (m)
D	circular obstacle diameter (μm)
D_i	kinematic diffusion coefficient ($\text{m}^2 \text{s}^{-1}$)
DG	diglycerides (-)
E	ethyl ester (-)
g	gravity acceleration (m s^{-2})
GL	glycerol (-)
k	reaction rate constants ($\text{m}^3 \text{mol}^{-1} \text{s}^{-1}$)
L_e	entrance length (μm)
L_m	mixing channel length (μm)
L_1	internal distance (μm)
L_2	external distance (μm)
M	mixing index (-)
MG	monoglycerides (-)
MSE	micromixer with static elements
MTB	micromixer with triangular baffles
M_W	molecular weight (kg kmol^{-1})
N_i	shape function value (-)
p	pressure ($\text{kg m}^{-1} \text{s}^{-2}$)
PI	performance index
$-r$	reaction rate ($\text{mol m}^{-3} \text{s}^{-1}$)
Re	Reynolds number (-)
S	mass source ($\text{kg m}^{-3} \text{s}^{-1}$)
TG	triglycerides (-)
u	uniform velocity normal to boundary inlet (m s^{-1})
<i>Greek symbols</i>	
μ	dynamic viscosity (Pa s)
v	stoichiometric coefficient of species (-)
β_o	data average
β_i	linear coefficients of regression
β_{ii}	quadratic coefficients of regression
β_{ij}	second interaction coefficients
ΔP	pressure drop
ν	kinematic viscosity ($\text{m}^2 \text{s}^{-1}$)
ρ	specific mass (kg m^{-3})
σ	mass fraction variance (-)
Φ	transport property (-)
<i>Subscripts</i>	
e	entrance
i	chemical species
m	mixing
w	width

enlarging, stating that the channel size can be increased up to a scale higher enough to achieve the desired performance, fundamentally keeping the microscale advantages of fast mixing and high heat and mass transfer rates. The channel dimensions increment affects the mixing quality and species dispersion, resulting in the decrease of fluid mixing and chemical reaction efficiency [11–13]. A comprehensive understanding of the microscale effects on the fluid flow is an essential step for the microdevice development and optimization. Several experimental and numerical studies were developed aiming the elucidation of the fluid flow and mixing process in microdevices. The most influential operating conditions and geometric variables on the micro-device performance were discussed, including the channel cross section (height/width ratio), fluid velocity, flow regimes and presence of micromixers [14–21]. These aspects, one of the most important aspects is the micromixer. A common element in microdevices with the aim of increasing the efficiency of fluid mixing [22–26].

Since the flow in microdevices is usually in laminar regime, the

mass transfer is dominated by molecular diffusion. The increment of the surface contact area between the fluids and the diffusion path reduction enhances the chemical species mixing [18]. A mechanism used to achieve these goals is the lamination, consisting the subdivision of the mainstream in n sub-streams, and then rearranging these in a new single mainstream [27,28]. The fluid mixing improvement also can be assessed by the use of micromixers with channels with obstructions. Among these, circular obstruction are capable to perform an efficient fluid mixing, since it promotes the lamination and can also generate vortices, enhancing the chemical species interactions [29]. Another common micromixer design element is the use of convergent-divergent sections [27,28,30,31]. In convergent-divergent micromixers, the channel width, W , is reduced to a $W' < W$ and then increased again to W . This size alteration occurs along the entire channel. The diffusion path is reduced when the fluid flows through the narrow section. Furthermore, at this section the flow is accelerated, improving the advection contribution.

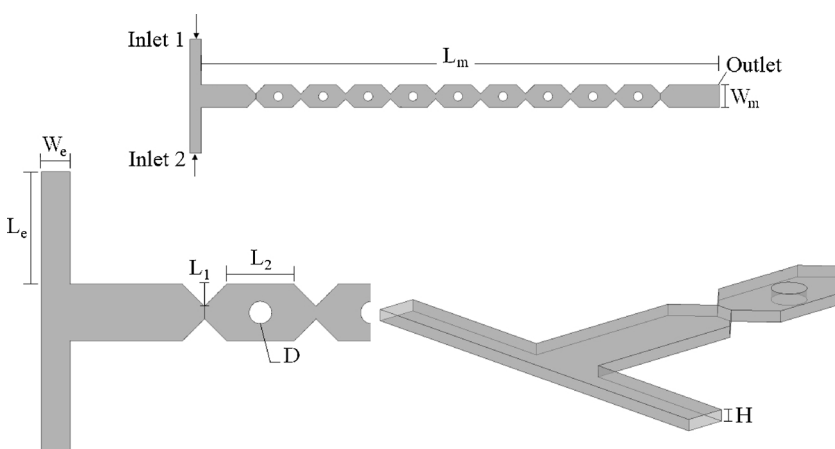


Fig. 1. Proposed design (MTB – micromixer with triangular baffles and circular obstructions) – the design variables were internal distance (L_1), circular obstacle diameter (D) and external distance (L_2). The channel geometric parameters were width (W_m), height (H) and longitudinal length (L_m). The entrance channel variables were length (L_e) and width (W_e).

Based on these mechanisms, a new design was proposed (MTB – micromixer with triangular baffles and circular obstructions), aiming efficient fluid mixing as micro- or milli-structured device. The new design consisted in convergent-divergent sections combined with circular obstacles, allowing the achievement of high mixing efficiency at low and high Reynolds numbers, independently of the scale, since presents the lamination, vortex generation and convergence-divergence mechanisms in a single device. The main goals of the present research were: (i) to evaluate the effects of the micromixer geometric variables on the mixing performance at the low Reynolds of 0.1 in order to obtain an optimized geometry based on mixing quality; (ii) to study the effect of Reynolds number on the oil/ethanol and water/ethanol mixing, comparing the performance of the new design with others from literature; (iii) to apply the new micromixer as a millireactor in the biodiesel synthesis.

2. Micromixer design and numerical investigation

The proposed micromixer (MTB – micromixer with triangular baffles and circular obstructions) is presented in Fig. 1. The design consists in triangular-shaped baffles and internal circular obstacles. The design geometric variables are: internal distance (L_1), circular obstacle diameter (D) and external distance (L_2). The channel width and height are W_m and H, respectively. The channel entrance length (L_e) and width (W_e) were $2W_m$ and $0.5W_m$, respectively. The total longitudinal length of the mixing microchannel was $3.51 \times 10^4 \mu\text{m}$. The geometries and numerical grids were created using the ANSYS ICEM 17.0.

A Central Composite Rotatable Design (CCRD) was used to evaluate the effect of internal distance (L_1), circular obstacle diameter (D) and external distance (L_2) on the fluid mixing performance. The geometric values were defined based on the literature and are summarized in Table 1. The fluid mixing response was modeled using a second-order polynomial equation, as given by Eq. 1:

$$M = \beta_0 + \beta_1 x_1 + \beta_2 x_2 + \beta_3 x_3 + \beta_{12} x_1 x_2 + \beta_{13} x_1 x_3 + \beta_{23} x_2 x_3 + \beta_{11} x_1^2 + \beta_{22} x_2^2 + \beta_{33} x_3^2 \quad (1)$$

where M is the response variable (mixing index), β_0 is the data average, β_i and β_{ii} are the linear and quadratic regression coefficients, respectively, β_{ij} are the second interaction coefficients and x_1 , x_2 and x_3 are the analyzed variables (design geometric parameters). The statistical data analysis was accomplished in Statistica 7 software.

All numerical runs were performed using the mathematical model experimentally validated in previous studies [7,21,32], detailed in the Appendices. The micromixer optimization was performed using a Central Composite Rotatable Design (CCDR) for the oil/ethanol flow at $Re = 0.1$, due to the distinct physicochemical properties and low miscibility of these fluids.

The effect of the Reynolds number was studied ranging the Reynolds number from 0.01 to 200 for the oil/ethanol flow and 0.1–100 for the water/ethanol flow. The biodiesel synthesis by vegetable oil transesterification with ethanolic solution of NaOH was chose to evaluate the MTB performance as a millireactor. This synthesis was defined due to the strong correlation of the reaction efficiency with the reactants mixing quality. The biodiesel synthesis was performed at 50°C , ethanol/oil molar ratio of 9 and catalyst concentration of 1.00% w/w (optimal reaction condition obtained by Santana et al. [7] and Santana et al. [33]) for residence times from 10 to 180 s. The results from

Reynolds number influence on mixing and chemical reaction performance were compared with literature results.

2.1. Mixing index (M), performance index (PI) and reaction efficiency

The micromixer performance was evaluated using the mixing index, the performance index and the vegetable oil conversion. The mixing degree between the fluid 1 (sunflower oil or water) and the fluid 2 (ethanol) was determined based on the mass fraction standard deviation of the fluid 1 in a cross section normal to the flow direction, according to Equation 2:

$$\sigma = \sqrt{\frac{\sum (Y_i - \bar{Y})^2}{N}} \quad (2)$$

where σ is the mass fraction variance, Y_i is the mass fraction at sampling point i , \bar{Y} is the mass fraction average and N is the number of sampling point in the cross section plane (over 1000 for the present study). The fluid mixing efficiency was calculated from Equation 3:

$$M = 1 - \sqrt{\frac{\sigma^2}{\sigma_{max}^2}} \quad (3)$$

where M is the mixing index and σ_{max}^2 is the maximum variance over the data interval (mass fraction variance in a cross section plane at fluid inlet). The mixing index is a unity for complete fluid mixing and zero for a complete segregation of the fluids.

The mixing efficiency was also evaluated using the Performance Index (PI). An efficient micromixer should provide high mixing index with lower pressure drop [14,27]. The PI is defined as the ratio of mixing index to the unit pressure drop required according to Equation 4:

$$PI = \frac{M}{\Delta P} \quad (4)$$

where ΔP is the pressure drop along the mixing channel, in Pa.

The oil conversion or the fraction of oil converted in products due to the chemical reaction was determined from Equation 5:

$$\text{Oil Conversion (\%)} = \left(\frac{C_{TG0} - C_{TGF}}{C_{TG0}} \right) \times 100 \quad (5)$$

where C_{TG0} is the initial oil concentration (at Inlet 2) and C_{TGF} is the final oil concentration (at Outlet).

2.2. Independence numerical mesh test

Before the mixing and chemical reaction analysis, a numerical mesh test was performed in order to reduce the influence of the spatial discretization on the predictions. The numerical mesh test was carried out for sunflower oil and ethanol at 25°C . The transport properties of the fluids were: sunflower oil specific mass = 914.96 kg m^{-3} ; ethanol specific mass = 786 kg m^{-3} ; sunflower oil dynamic viscosity = 0.055 Pa.s ; ethanol dynamic viscosity = 0.0011 Pa.s . Uniform velocities ($U = 17 \text{ m/s}$) were employed as inlet boundary conditions for both fluids ($Re = 100$, considering the channel of dimensions $W_m = 1500 \mu\text{m}$ and $H = 200 \mu\text{m}$). The mixing index predicted by the different grid refinement level was compared and are shown in Fig. 2.

Significant differences in the meshes predictions were observed in the axial position of the channel from 5 to 20 mm. At the channel outlet, all meshes predicted same mixing indexes. The grid spatial discretization independence was observed for the mesh composed by 3.0×10^6 elements, since it presented the closest results from the most refined grid (4.0×10^6 control volumes). Based on this, the grid composed by 3.0×10^6 elements was used in the mixing and chemical reaction studies.

Table 1
CCDR variable values for the three geometric parameters evaluated.

Variable	Code	-1.68	-1	0	1	1.68
Internal Distance (L_1) (μm)	x_1	500	533.2	582	622.5	650
Obstacle Diameter (D) (μm)	x_2	300	421	600	897.6	1100
External Distance (L_2) (μm)	x_3	1300	1502.3	1800	1978.6	2100

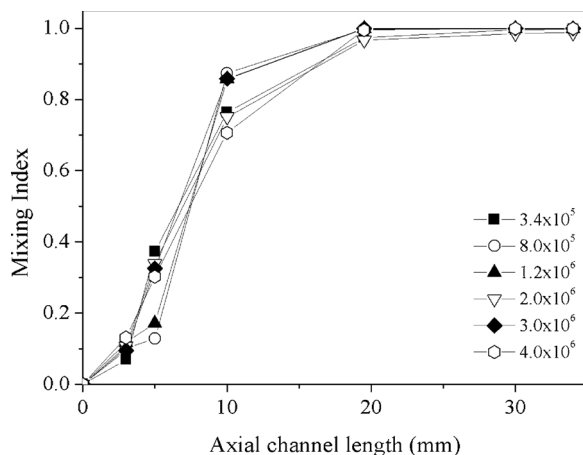


Fig. 2. Independence mesh test results for different grid refinements at $Re = 100$ (Channel width = 1500 μm ; Height = 200 μm ; Internal Distance = 582 μm ; Obstacle Diameter = 600 μm ; External Distance = 1800 μm).

3. Results and discussion

In the previous section a new micromixer design composed by triangular baffles and circular obstacles was proposed for fluid mixing and chemical reactions processing in millidevices. The numerical investigation results are presented following.

3.1. Optimization of MTB micromixer geometric variables

In order to evaluate the influence of internal distance (L_1), obstacle diameter (D) and external distance (L_2) on the oil-ethanol mixing in low Reynolds number ($Re = 0.1$), a CCRD (2^3) with 15 numerical runs was accomplished. **Table 2** summarizes the mixing index results. The mixing index (M) ranged from 0.327 to 0.515 for the operating range evaluated. From these results, the effect of each geometric variable on the fluid mixing was estimated, as presented in **Table 3**.

From **Table 3**, it was noticed that the average, and the linear terms of internal distance ($x_1 - L_1$) and obstacle diameter ($x_2 - D$) were statistically significant at 5% ($p\text{-value} < 0.05$). The variation explained by the statistical model was 91.78%. The mixing index at Reynolds number of 0.1 was influenced mostly by the internal distance and obstacle diameter.

The increment of the internal distance (x_1) provides an enhancement of fluid mixing. As previously explained, at very low Reynolds numbers, the fluid flow in microchannels/micromixers are characterized by deep laminar flow (the fluid motion is marked by fluid layers flowing in the absence of macromixing). Therefore, the species mixing occurs exclusively by molecular diffusion. The increase on internal distance provides a decrease in channel width (channel throttling), decreasing the diffusing path, enlarging the contact between the fluids and consequently enhancing the fluid mixing. The larger internal distance, greater is the diffusion path reduction. As examples, in case 10 from **Table 2** ($L_1 = 650 \mu\text{m}$) means that the fluid stream flowing through the throttling, the channel width was reduced from 1.5 mm (millidevice scale) to 200 μm (microdevice scale). In this zone, the mixing process experiences the microscale characteristic.

The increment of obstacle diameter (x_2) also resulted in higher mixing indexes. The circular obstacles split the main fluid stream in sub-streams. This mechanism is also accompanied for the diffusion path reduction, increasing the chemical species contact. Larger obstacle diameters result in narrower sub-streams, consequently enhancing the contact area between the fluids. The mixing processes induced by the MTB design at low Reynolds number are illustrated in **Fig. 3**.

Fig. 4 shows the good agreement of mathematical model to the

predicted results. Equation 6 gives the adjusted statistical model with codified terms (x_1 , x_2 and x_3):

$$M = 0.371 + 0.042x_1 + 0.018x_1^2 + 0.023x_2 + 0.010x_2^2 + 0.007x_3 + 0.001x_3^2 - 0.003x_1x_2 - 0.002x_1x_3 - 0.003x_2x_3 \quad (6)$$

In **Fig. 5**, the mixing index behavior in function of internal and external distance variation was provided by the mathematical model given by Equation 6. The highest mixing indexes were obtained from the maximum distances of the pre-determined range. The optimal geometric parameters, defined as the internal distance (x_1), obstacle diameter (x_2) and external distance (x_3), obtained from the statistical model for the Reynolds number of 0.1 are summarized in **Table 4**. The mixing index predicted by both models, statistical model (Equation 6) and CFD model, using the optimal values for x_1 , x_2 and x_3 are also given in **Table 4**. From these results, the deviation between the statistical model and the CFD prediction were 5.62%, showing good agreement. Thus, it can be concluded that the model presented in Equation 6 can be used to relate the optimization parameters, i.e., internal distance (x_1), obstacle diameter (x_2) and external distance (x_3), with geometries with dimensions not used here, allowing the development of microdevices using the MTB to other processes not mentioned here, provided that the values coded for x_1 , x_2 and x_3 are within the interval considered (**Table 1**).

In this section the effects of the proposed geometric variables on the oil-ethanol fluid mixing process and the CCRD application on geometric optimization were demonstrated. The mixing index value predicted for the optimal geometry ($M = 0.587$, from **Table 4**) can be compared with the mixing index obtained by Santana et al. [7] for the MSE micromixer (micromixer with static elements disposed perpendicularly along the longitudinal length with channel width of 1.5 mm, channel height of 200 μm). The MSE design provided high oil/ethanol mixing indexes, mostly for elevated Reynolds numbers. For $Re = 0.1$ the MSE micromixer yield a mixing index of 0.413. This comparison shows a significant mixing index enhancement of 42% achieved by the MTB micromixer.

In the next sections, the application of the MTB for sunflower oil/ethanol and water/ethanol mixing ranging the Reynolds number is demonstrated. Moreover, the use of the MTB as a millireactor for biodiesel synthesis is exposed.

3.2. Effect of Reynolds number on oil/ethanol mixing

The mixing index obtained from the Reynolds number range of 0.01 to 200 is presented in **Fig. 6**, considering a channel width (W) of 1500 μm and different heights (H). High mixing indexes ($M = 0.99$) were observed for all investigated channel heights. For the heights of

Table 2
Codified variable value* and obtained mixing index.

Run	x_1 (L_1 - μm)	x_2 (D - μm)	x_3 (L_2 - μm)	M
1	-1 (533.2)	-1 (421)	-1 (1502.3)	0.330
2	+1 (622.5)	-1 (421)	-1 (1502.3)	0.416
3	-1 (533.2)	+1 (897.6)	-1 (1502.3)	0.380
4	+1 (622.5)	+1 (897.6)	-1 (1502.3)	0.438
5	-1 (533.2)	-1 (421)	+1 (1978.6)	0.370
6	+1 (622.5)	-1 (421)	+1 (1978.6)	0.430
7	-1 (533.2)	+1 (897.6)	+1 (1978.6)	0.393
8	+1 (622.5)	+1 (897.6)	+1 (1978.6)	0.458
9	-1,68 (500)	0 (600)	0 (1800)	0.327
10	+168 (650)	0 (600)	0 (1800)	0.515
11	0 (582)	-1,68 (300)	0 (1800)	0.340
12	0 (582)	+168 (1100)	0 (1800)	0.455
13	0 (582)	0 (600)	-1,68 (1300)	0.369
14	0 (582)	0 (600)	+168 (2100)	0.373
15	0 (582)	0 (600)	0 (1800)	0.372

*Real variable values are provided between parentheses.

Table 3
Variables effects on mixing index.

Factor	Effects	Std. Deviation	t(5)	p-value	Interval Estimative (95%)	
					Inferior limit	Superior limit
Average	0.371	0.025	14.580	0.00003	0.305	0.436
x_1 (L)	0.086	0.014	6.199	0.002	0.050	0.121
x_1 (Q)	0.037	0.021	1.767	0.137	-0.017	0.090
x_2 (L)	0.046	0.014	3.344	0.020	0.011	0.082
x_2 (Q)	0.021	0.021	0.994	0.366	-0.033	0.074
x_3 (L)	0.014	0.014	0.977	0.374	-0.022	0.049
x_3 (Q)	0.002	0.021	0.073	0.945	-0.052	0.055
x_1x_2	-0.006	0.018	-0.327	0.757	-0.052	0.041
x_1x_3	-0.005	0.018	-0.259	0.806	-0.051	0.042
x_2x_3	-0.005	0.018	-0.299	0.777	-0.052	0.041

% explained variation (R^2) = 91.78; (L) – linear; (Q) – quadratic.

200 μm and 1000 μm this maximum mixing index was noticed at $Re = 10$, while, for height of 2000 μm it was achieved only at $Re = 100$. A zone of decreasing of mixing index until the minimum was observed for all channel heights at $Re = 0.1$. The minimum mixing index was noticed for the height of 2000 μm ($M = 0.195$ at $Re = 0.1$). This point of minimum mixing index splits the fluid mixing profile in two well-defined distinct regions: the molecular diffusion predominance and the advection dominant zone.

In the first zone, only the molecular diffusion is responsible for the mixing process and with smaller Reynolds number (lower speed), the molecules experience longer times to diffuse, i.e., the chemical species has longer residence time to move to the opposite side of the channel, increasing the mixing efficiency. Moreover, the MTB design favors the molecular diffusion by the diffusion path reduction, as previously explained (see Fig. 3). In Table 2, the higher mixing index was 0.515 ($Re = 0.1$, $W = 1500 \mu\text{m}$ and $H = 200 \mu\text{m}$). For $Re = 0.01$, the mixing indexes were 0.681, 0.877, 0.710 and 0.654 (Fig. 6), for the heights of 200 μm , 400 μm , 1000 μm and 2000 μm , respectively.

As observed, the minimum mixing index was noticed at $Re = 0.1$. This behavior can be attributed to the velocity increment, relative to $Re = 0.01$, decreasing the fluid residence time in the device. Once the $H = 2000 \mu\text{m}$ presents the smallest interfacial area among the studied geometries, this height resulted in the lowest mixing index. Beyond the minimum point at $Re = 0.1$, the mixing index increased with the Reynolds number for all channel heights. The increment of mixing index in this region can be attributed to the advection mechanism.

As the velocity increases, with the Reynolds number increment, the fluids experience short contact times, and then, the molecular diffusion becomes less influential in the mixing process. However, the velocity increment promotes disturbances on the fluid motion, enhancing the

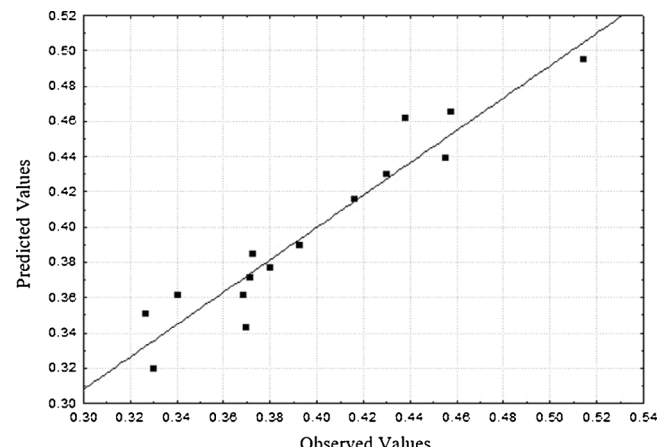


Fig. 4. Observed and predicted mixing index values from the mathematical model.

chemical species interaction, counterbalancing the efficiency loss of diffusion mechanism [28]. The mixing index presented a minimum at $Re = 0.1$, increasing at $Re = 1$. At this point, the advection predominance zone was observed. In Fig. 6, this advection zone promoted an increase in the mixing index up to a maximum of 0.99 for all channel heights.

In addition to the flow disturbances, the mixing efficiency enhancement also is a result from the presence of circular obstacles in the mixing channel. The circular obstacles modify the flow direction from the channel throttling. These direction changes lead to vortex formation, enhancing the mixing efficiency. The vortex generation in the MTB

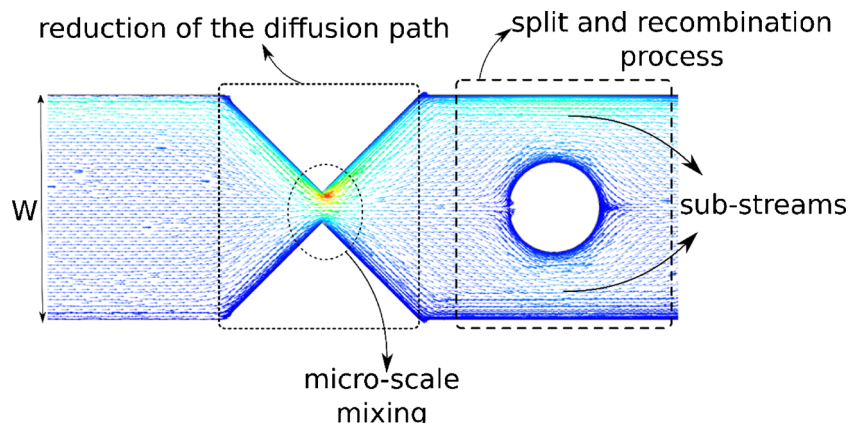


Fig. 3. Mixing processes presented in the MTB at low Reynolds number – Case 10 from Table 2 (Internal distance of 650 μm ; obstacle diameter of 600 μm ; external distance of 1800 μm).

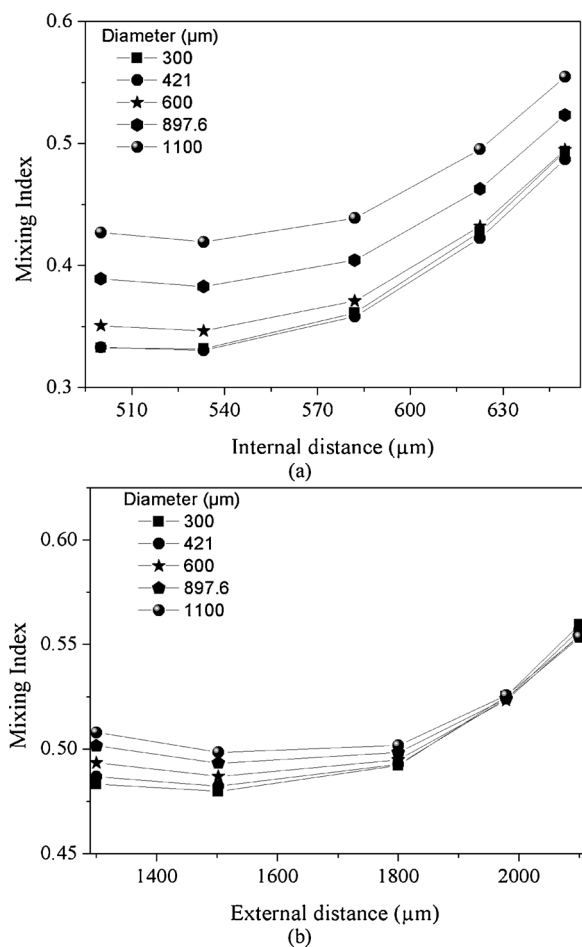


Fig. 5. Mixing index variation predicted by the statistical model: (a) mixing index dependence on the internal distance and obstacle diameter for a fixed external distance of 1800 μm ; (b) mixing index dependence on external distance and obstacle diameter for a fixed internal distance of 650 μm .

Table 4

Optimized geometric parameters and predicted mixing index from statistical model and CFD simulation.

Geometric parameter	Real value	Codified value
Internal distance (μm)	650	+1.68
Obstacle diameter (μm)	1100	+1.68
External distance (μm)	2100	+1.68
Mixing index (M)	0.554	CFD result
Deviation (%)	5.62	

is dependent on Reynolds number, i.e., the stream velocity. The main difference of the proposed MTB design is that the vortex generation already starts in $\text{Re} = 10$, as observed in Fig. 7.

At $\text{Re} = 1$, the fluid flow bypasses the circular obstacles softly (Fig. 7). The fluid mixing occurs by channel width reduction (convergence zone) and mainstream division in sub-streams (Fig. 3). At $\text{Re} = 10$, the vortex formation starts, acting as an intense mixing process. The zone of reverse flow enhances the local mass transfer rate. The reverse flow was observed only in the obstacle incoming zone for the $\text{Re} = 10$. At $\text{Re} = 100$, the vortex generation was observed in both, incoming and outgoing zones from the obstacle. This phenomenon was not significant on the performance for high interfacial areas (heights of 200 μm , 400 μm , 1000 μm). However, for the channel height

of 2000 μm , the vortex generation in both obstacles sides was necessary to achieve $M = 0.99$.

After the evaluation of the channel height on the mixing index, the channel width was ranged (1500 μm , 2000 μm and 3000 μm) for a fixed height of 400 μm . The geometric scale ratio was employed in order to maintain the optimal dimensions proportion, as listed in Table 4. As example, for a width of 3000 μm , the geometric scale ratio was 3000/1500 = 2. Accordingly, all dimensions of the MTB design (internal distance, obstacle diameter and external distance) were multiplied by the factor of 2. Similar procedure was performed for the channel width of 2000 μm . The predicted mixing indexes for the scaled geometries are shown in Fig. 8.

In Fig. 8, the distinct zones of mass transfer mechanism predominance (diffusion or advection) were also observed as in Fig. 6. For this case, the distinction between the zones was better defined. An elevated efficiency occurred in very low Reynolds number ($\text{Re} = 0.01$), due to the molecular diffusion predominance. The increment in Reynolds numbers led to a minimum mixing index, and then, further increase in the velocity favored the advection, counterbalancing the lower effect of an effective molecular diffusion mechanism in the mixing process. High mixing indexes (0.99) were observed for all channel widths for $\text{Re} \geq 10$.

Once the mixing index dependence on channel dimensions (width and height) was presented, the performance index (PI) was evaluated for all geometries. The PI quantifies the ratio of mixing efficiency to the unit pressure drop required, i.e., a high value of PI indicates good performance of the micromixer. The PI results for all geometries are summarized in Table 5.

The superior PI of 1.13×10^{-2} was exhibited by the geometry W1500H2000 (channel width of 1500 μm and height of 2000 μm , $d_H = 1714.3 \mu\text{m}$) at $\text{Re} = 0.01$. The PI decreased with the Reynolds number increment for all geometries (Table 5), presenting a maximum at the very low $\text{Re} = 0.01$. The increment of Reynolds number resulted in the pressure drop increase, due to the considerable increment of velocity.

The geometries with superior performance were W1500H1000, W1500H2000 and W3000H400. Among these, the W1500H2000 presented superior performance in practically all Reynolds numbers. This performance was attributed to the lower pressure drop regarding the other geometries. The pressure drop in the W1500H2000 varied from 99.59 Pa ($\text{Re} = 0.01$) to 1.52×10^7 Pa ($\text{Re} = 200$). The geometry W1500H2000 provided a mixing index of 0.71 at $\text{Re} = 0.01$. The geometry W3000H400 ($d_H = 705.9 \mu\text{m}$) exhibited a mixing index of 0.92 at $\text{Re} = 0.01$, with a pressure drop of 242.64 Pa. At $\text{Re} = 200$, the pressure drop of the geometry W3000H400 was 9.7×10^7 Pa. Based on this, the geometry W3000H400 presented superior performance.

After choosing the optimal geometry (W3000H400), the effect of the number of baffles in the mixture performance was carried out. Fig. 9 shows the variation of the mixing index as a function of the mixing unit (i.e., one mixing unit comprises two sections of channel throttling). Fig. 9 shows the mixing index increment with the number of mixing units for all Reynolds numbers, mainly at $\text{Re} = 0.01$ and $\text{Re} = 0.1$. For Reynolds equal to 10 and 100, the number of mixing units required to achieve the maximum mixing index were 5 and 4, respectively. The behavior agreed with the zones of mass transfer mechanism predominance (diffusion or advection), observed in Figs. 6 and 8. The diffusion and the advection contributed to the mixing indexes increment, and the perturbation of the flow (advection) contributed to a reduction in the number of units needed to achieve the highest degree of mixing ($\text{Re} = 10, 100$), as observed in Fig. 10.

Table 6 shows the performance index (PI) as a function of the mixing unit. The PI decreased with the increase of the number of mixing units, due to the increment in the pressure drop with the number of

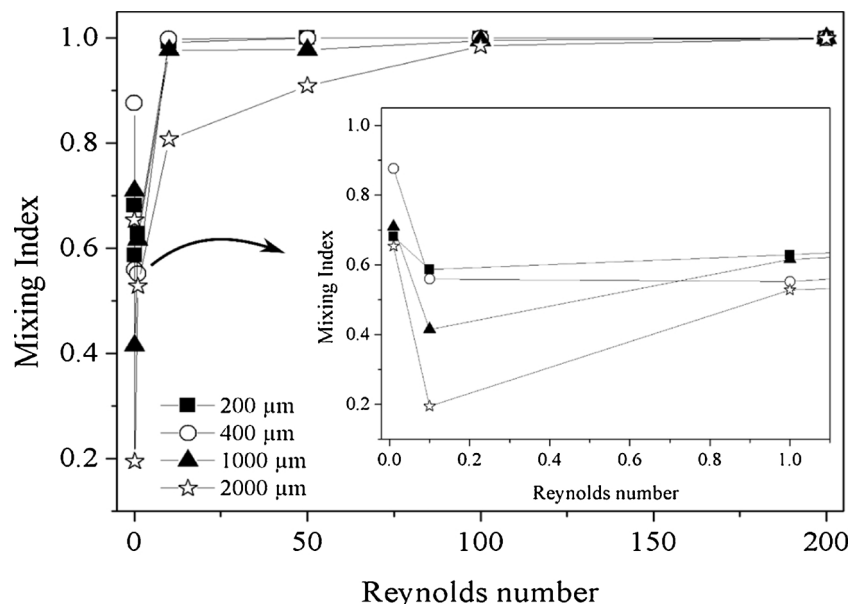


Fig. 6. Mixing index as a function of Reynolds number for different micro- and millichannel heights. The channel width was 1500 μm .

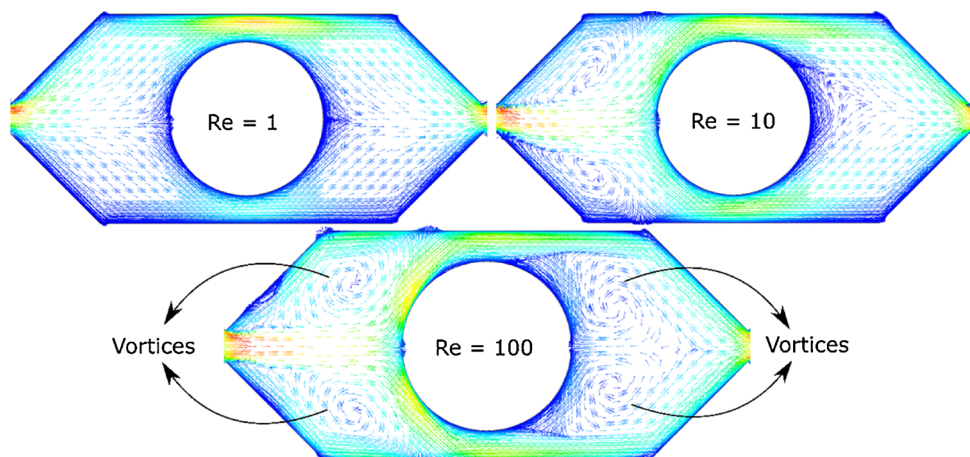


Fig. 7. Vector field for velocity for Reynolds numbers of 1, 10 and 100 – (channel width = 1500 μm ; height = 400 μm ; internal distance = 650 μm ; diameter = 600 μm ; external distance = 1800 μm). The vector field was plotted at a plane located at the half-height of the channel.

units. The increment of the Reynolds number resulted in a reduction of the MTB performance. Although in higher Reynolds numbers the highest mixing indexes were obtained (Fig. 9), the highest pressure drops also were noticed influencing directly the micromixer performance index. Accordingly, the optimal operating condition was at $\text{Re} = 0.01$ (superior mixing performance at lower pressure drops).

Fig. 11 presents the comparison between the geometry W3000H400 with the micromixer MSE [7] operating with the same fluids. MSE has dimensions of channel width of 1500 μm , height of 200 μm and $d_H = 353 \mu\text{m}$. MTB W3000H400 presents $d_H = 706 \mu\text{m}$. Smaller hydraulic diameters provides larger interfacial areas and shorter molecular diffusion paths, consequently, superior fluid mixing can be achieved in channels with larger interfacial areas. This expected tendency was not observed comparing the MSE with the MTB. Even with a double hydraulic diameter size, MTB exhibited higher mixing index at low Reynolds numbers. The mixing index at $\text{Re} = 0.1$ were 0.56 (MTB) and 0.41 (MSE), and at $\text{Re} = 1$ were 0.602 (MTB) and 0.43 (MSE) (Fig. 11a). For Reynolds number above 10, the mixing indexes provided by both micromixers were equal. Comparing the performance index, the MTB presented a PI three times superior than MSE at $\text{Re} = 0.01$, even with a larger hydraulic diameter. These

results highlight the efficiency of the MTB even with larger dimension sizes regarding other micromixer designs.

3.3. MTB as millireactor

In the previous section an optimal geometry for the MTB design was defined bases on the mixing index. In the present section the optimal MTB geometry was used as a millireactor in the biodiesel synthesis. The sunflower oil transesterification with ethanol and sodium hydroxide was carried out, since this process yield is directly correlated with the fluid mixing degree [34], allowing the millireactor performance evaluation. Fig. 12 presents the sunflower oil conversion (Fig. 12a) and the ethyl ester (biodiesel) outlet concentration (Fig. 12b) as a function of the residence time.

The increment in residence time from 10 s to 30 s resulted in a sunflower oil conversion increase (Fig. 12a). For a residence time of 10 s, the oil conversion was 78.01%. The maximum oil conversion of 92.67% was obtained for a residence time of 30 s. From the literature, it was demonstrated that with the increment of residence time, the triglycerides and ethanol molecules has sufficient time to react and the

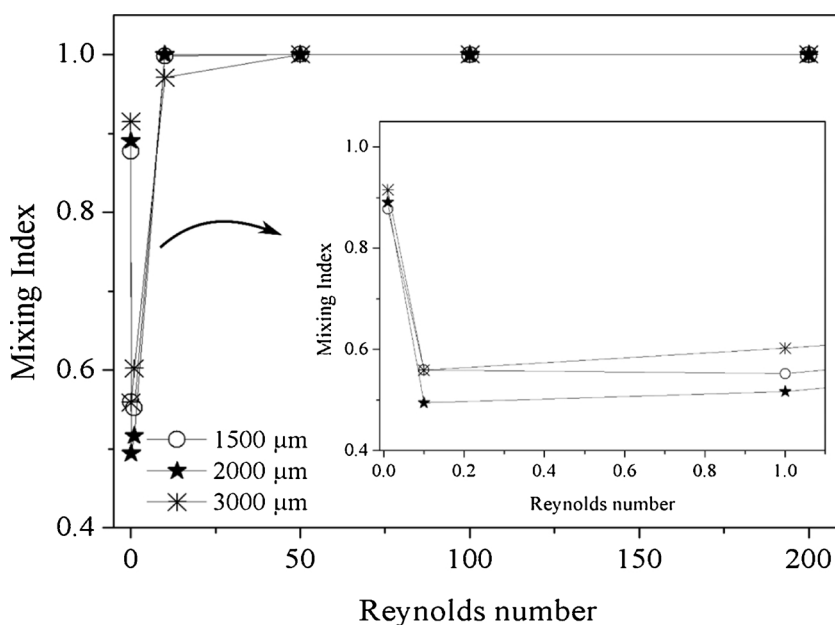


Fig. 8. Mixing index dependence on Reynolds number for different channel widths. The channel height was 400 μm . The geometry dimensions for the width of 2000 μm were: internal distance (L_1) (μm) = 866.45; diameter (D) (μm) = 1466.3; external distance (L_2) (μm) = 2799.3; entrance channel width (μm) = 1000. The geometry dimensions for the width of 3000 μm were: internal distance (L_1) (μm) = 1300; diameter (D) (μm) = 2200; external distance (L_2) (μm) = 4200; entrance channel width (μm) = 1500.

chemical reaction would be virtually complete at the channel outlet [35–37]. Moreover, longer residence times favor the molecular diffusion, resulting in a greater uniformity of the species along the channel. This phenomenon occurred in the MTB considering the residence time range of 10 s to 30 s.

A reduction on the oil conversion was observed for longer residence times (60 s – 180 s). As the transesterification reaction is a reversible chemical reaction, longer contact times can displace the reaction preference, favoring the reverse step towards the reactants, producing fewer biodiesel, as observed in Fig. 12b. The maximum biodiesel yield was observed for a residence time of 30 s, decreasing for longer residence times. Accordingly, for the considered operating conditions ($T = 50^\circ\text{C}$, ethanol/oil molar ratio of 9, catalyst concentration of 1.0% w/w), the optimum residence time was 30 s.

A comparison of the MTB millireactor with other microdevices with similar longitudinal length of 35 mm was made and is summarized in Table 7. MTB provided the superior oil conversion among the evaluated microreactors, even with the hydraulic diameter twice larger, and channel width characteristic of a millichannel, standing out the efficiency of the proposed design.

3.4. Effect of Reynolds number on water/ethanol mixing

In the previous sections, the MTB efficiency was evaluated for oil/

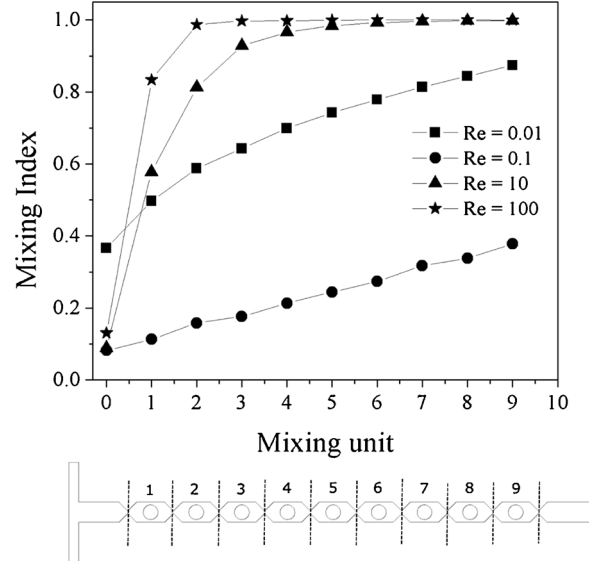


Fig. 9. Mixing Index as a function of the number of mixing units for different Reynolds numbers (micromixer MTB W3000H400 - channel width of 3000 μm and channel height of 400 μm).

Table 5

Effects of channel width (W) and height (H) on Performance Index for all Reynolds number range of oil/ethanol flow.

Geometry	Hydraulic diameter, d_H (μm)	Performance Index (PI) for oil/ethanol flow						
		Reynolds Number						
		0.01	0.1	1	10	50	100	200
W1500H200	353	6.78×10^{-4}	5.89×10^{-5}	6.02×10^{-6}	5.46×10^{-7}	3.58×10^{-8}	9.92×10^{-9}	2.66×10^{-9}
W1500H400	632	2.94×10^{-3}	2.06×10^{-4}	1.96×10^{-5}	1.90×10^{-6}	1.18×10^{-7}	3.23×10^{-8}	8.45×10^{-9}
W1500H1000	1200	7.12×10^{-3}	4.19×10^{-4}	6.35×10^{-5}	6.29×10^{-6}	4.08×10^{-7}	1.19×10^{-7}	3.13×10^{-8}
W1500H2000	1714	1.13×10^{-2}	3.13×10^{-4}	8.54×10^{-5}	9.34×10^{-6}	8.12×10^{-7}	2.46×10^{-7}	6.57×10^{-6}
W2000H400	667	3.49×10^{-3}	2.03×10^{-4}	2.03×10^{-5}	2.09×10^{-6}	1.30×10^{-7}	3.58×10^{-8}	9.30×10^{-9}
W3000H400	706	3.77×10^{-3}	2.38×10^{-4}	2.44×10^{-5}	2.22×10^{-6}	1.45×10^{-7}	3.94×10^{-8}	1.03×10^{-8}

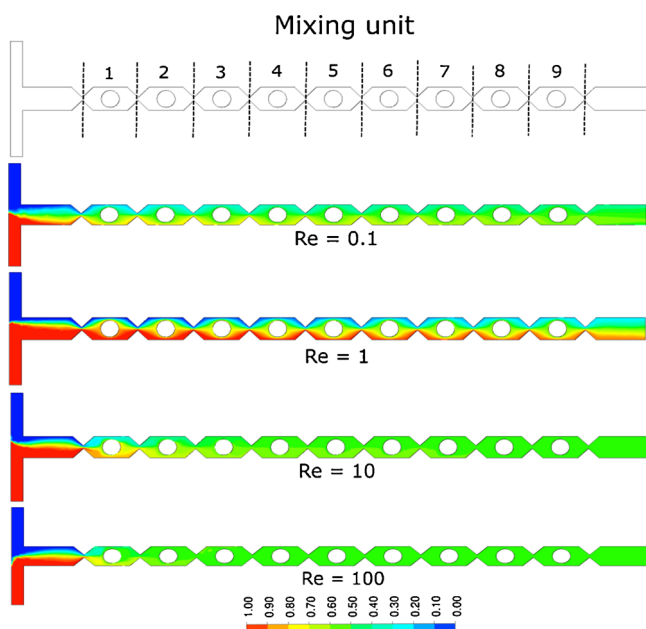


Fig. 10. Oil mass fraction distribution for different Reynolds numbers.

Table 6
Effect of the number of mixing units on the Performance Index at different Reynolds numbers.

Mixing unit	Performance Index (PI) for oil/ethanol flow				
	Reynolds Number	0.01	0.1	10	100
1		13.9×10^{-3}	3.36×10^{-4}	7.16×10^{-6}	17.1×10^{-8}
2		9.66×10^{-3}	2.78×10^{-4}	6.50×10^{-6}	13.2×10^{-8}
3		7.47×10^{-3}	2.18×10^{-4}	5.38×10^{-6}	9.90×10^{-8}
4		6.28×10^{-3}	2.03×10^{-4}	4.49×10^{-6}	7.95×10^{-8}
5		5.44×10^{-3}	1.89×10^{-4}	3.77×10^{-6}	6.59×10^{-8}
6		4.81×10^{-3}	1.78×10^{-4}	3.24×10^{-6}	5.64×10^{-8}
7		4.35×10^{-3}	1.77×10^{-4}	2.83×10^{-6}	4.94×10^{-8}
8		3.98×10^{-3}	1.66×10^{-4}	2.52×10^{-6}	4.36×10^{-8}
9		3.69×10^{-3}	1.65×10^{-4}	2.26×10^{-6}	3.93×10^{-8}

ethanol mixing and as a biodiesel synthesis millireactor. In the present section, the mixing efficiency for the water/ethanol is presented. Usually, binary systems with similar transport properties are found in literature in the micromixer performance evaluation. The MTB geometry W1500H200 was used, once the mixing process is often performed in devices with the smallest allowed dimensions of cross section and longitudinal length. The mixing and performance indexes profiles over the evaluated Reynolds number range are presented in Fig. 13.

High mixing indexes (0.99) were observed at low Reynolds number ($Re = 0.1$) and at the higher Reynolds numbers of 50 and 100 (Fig. 13a). The mixing index profile was similar to the observed in Figs. 6 and 8, with a clear distinction between molecular diffusion and advection predominance zones. At $Re = 0.1$, the mixing index was 0.99, while at $Re = 10$ was $M = 0.76$. Further increment on Reynolds number increased the mixing index to 0.99. The performance index profile was similar to the observed in Fig. 13b. The superior PI was 1.0×10^{-1} at $Re = 0.1$.

Table 8 presents a comparison about the proposed MTB millidevice with microdevices found in literature. Despite the scale-up of the MTB design to the milli scale, high mixing efficiencies compared to the microdevices were observed. In some cases, the MTB millichannel presented superior performance regarding the microdevices listed in

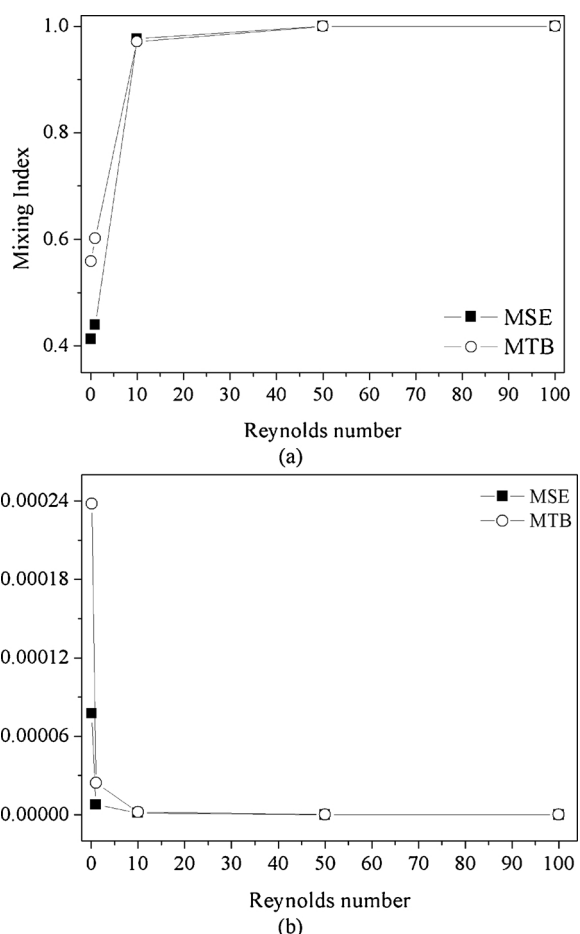


Fig. 11. Mixing index (a) and performance index (b) dependence on Reynolds number for the MSE ($d_H = 353 \mu\text{m}$) and MTB ($d_H = 706 \mu\text{m}$) micromixers.

Table 8. These results stand out the capability of high mixing performance of millidevices without missing the microscale transport properties.

An important aspect of the microdevices is the longitudinal length, once is recommended the use of reduced lengths. In this context, the MTB showed good performance, as illustrated in Fig. 14. At $Re = 0.1$ only 3.5 mm of longitudinal length was necessary to achieve a high mixing efficiency ($M \geq 0.90$). However, for higher Reynolds number, at least 10.5 mm were necessary ($Re = 100$). Accordingly, for operation in very reduced channel lengths, the water/ethanol mixture should be operated at $Re = 0.1$.

4. Conclusion

In the present study the high performance of millidevices in fluid mixing and chemical reaction conversion were demonstrated. A new micromixer design (MTB – micromixer with triangular baffles and circular obstructions) was proposed aiming the combination of three mass transfer enhancements mechanisms: reduction of molecular diffusion path, split and recombination of streams and vortex generation. This combination allows obtaining high mixing efficiency at low and high Reynolds numbers, independently of the scale. It has been demonstrated that the MTB allows high mixing efficiency, at various heights and mixing channel widths, and can be used in micrometric and millimeter scale.

Initially, the effect of the geometric variables was evaluated in order to define an optimized geometry. The optimal geometry dimensions

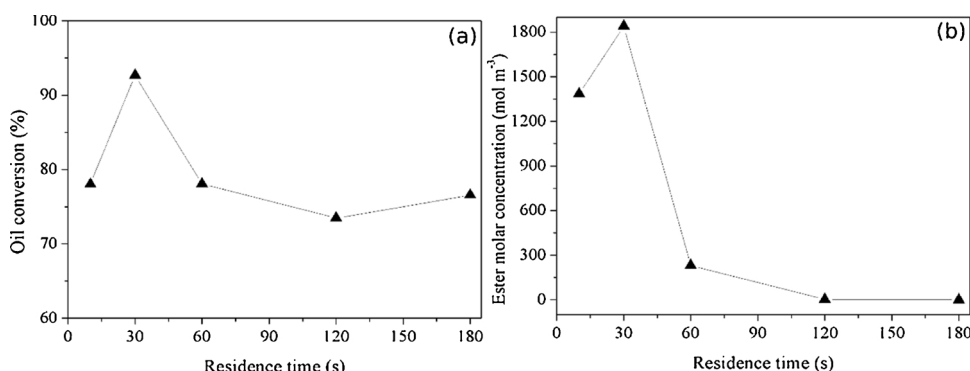


Fig. 12. Sunflower oil conversion (a) and biodiesel outlet molar concentration (b) as a function of residence time in the MTB – W3000H400 (width = 3000 μm , height = 400 μm).

Table 7

Comparison of the sunflower oil conversion performance in different micro-reactors with the MTB millireactor.

Reactor	T (°C)	Ethanol/Oil Molar Ratio	Catalyst Conc. (%)	Oil Conversion (%)	Reference
T-channel ^a	75	9	1	76.29	[33]
MCO ^b	75	9	1	81.13	[33]
MSE	75	9	1	91.53	[7]
MTB	50	9	1	92.67	Present

^a Micromixer without internal obstructions.

^b Micromixer with a set of three circular obstructions. Both presents channel width of 1500 μm , height of 200 μm , hydraulic diameter = 353 μm .

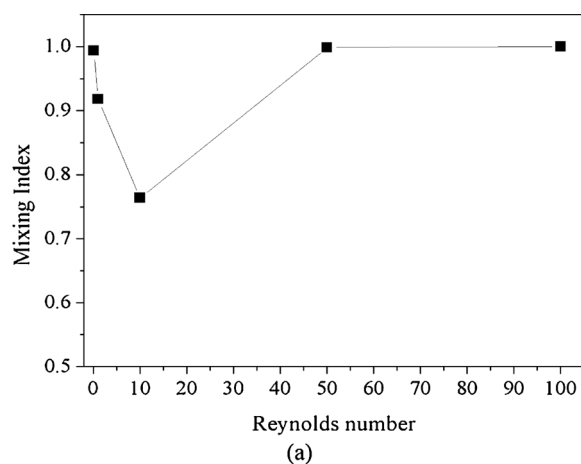


Fig. 13. Mixing index (a) and performance index (b) dependence on the Reynolds number for water/ethanol flow in the MTB - W1500H200 (width = 1500 μm , height = 200 μm).

Table 8

Mixing index (*M*) and performance index (*PI*) of different microdevices under a wide range of Reynolds numbers.

Fluids	<i>M</i>		<i>PI</i>		Reference
	Re = 1	Re = 50	Re = 1	Re = 50	
Water	0.55	0.93	$\sim 10^*$	$\sim 10^{-2}$	[38]
Water/Ethanol	0.15	0.5	–	–	[39]
Water/Ethanol	0.89	0.99	2×10^{-2}	10^{-3}	[27]
*	0.97	0.96	3.83×10^{-2}	31×10^{-5}	[14]
**	0.1	100	–	–	[20]
Water	~0.90	~0.93	–	–	[40]
Water	0.156	0.75	–	–	[41]
Water	~0.82	0.95	–	–	[42]
Water	~0.98	0.97	–	–	[43]
Water/Ethanol	0.70	1.00	–	–	[44]
Water/Ethanol	0.05	40	–	–	Present
Water/Ethanol	~0.80	~0.95	–	–	–
Water/Ethanol	0.99	0.99	1.0×10^{-1}	3.46×10^{-5}	–

* Fluid with transport properties of: $\rho = 998 \text{ kg m}^{-3}$, $\mu = 1 \times 10^{-3} \text{ kg m}^{-1}\text{s}^{-1}$, $D = 2.2 \times 10^{-9} \text{ m}^2 \text{s}^{-1}$; ** Fluid with transport properties of: $\rho = 10^3 \text{ kg m}^{-3}$, $\mu = 10^{-3} \text{ kg m}^{-1}\text{s}^{-1}$, $D = 10^{-9} \text{ m}^2 \text{s}^{-1}$; *** Fluid with transport properties of: $\rho = 10^3 \text{ kg m}^{-3}$, $\mu = 10^{-3} \text{ Pa s}$, $D = 10^{-11} \text{ m}^2 \text{s}^{-1}$; the symbol - means that no *PI* data were supplied.

were used in the fluid mixing performance evaluation for vegetable oil/ethanol and water/ethanol in the range of Reynolds numbers of 0.01–200 and for the process of biodiesel synthesis (vegetable oil transesterification with ethanol and NaOH). The micromixer performance was assessed by the mixing index (*M* – fluid mixing quality based on the distribution of the chemical species mass fraction), performance index (*PI* – ratio of mixing quality to the unit pressure drop required) and the vegetable oil conversion.

For the oil/ethanol flow, high mixing index (*M* = 0.99) was noticed for different channel dimensions (heights of 200 μm –2000 μm and widths of 1500 μm –3000 μm). The results of *M* aided the distinction of the mass transfer mechanism zones (molecular diffusion and advection). The superior *PI* of 1.13×10^{-2} was provided by the geometry W1500H2000 (channel width of 1500 μm and height of 2000 μm) at $Re = 0.01$ and a mixing index of 0.71. The geometry W3000H400 also presented low pressure drop, with the superior mixing index of 0.92 at $Re = 0.01$. Hence, the geometry W3000H400 was defined as optimal for the oil/ethanol mixing process and was compared with the MSE micromixer (Santana et al. [7]). The MTB mixing indexes were superior

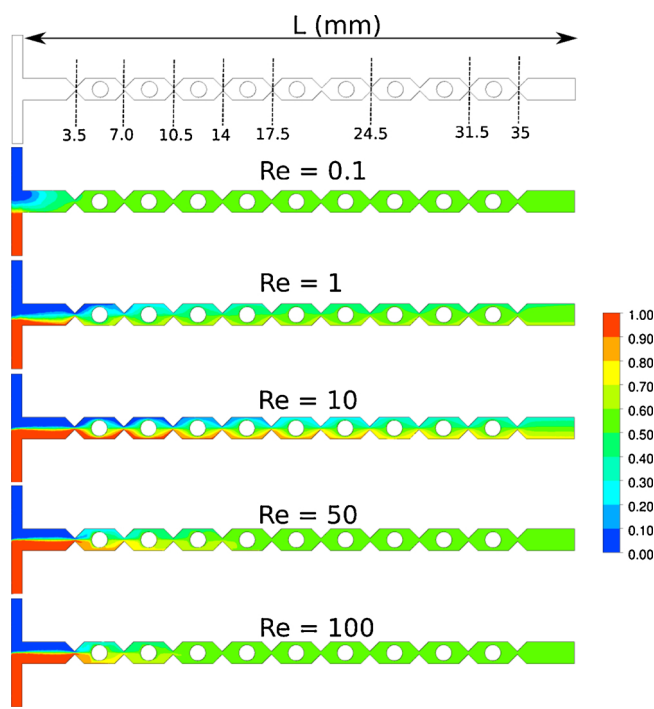


Fig. 14. Water mass fraction distribution for different Reynolds numbers.

than the MSE indexes at low Reynolds number, even with the MTB presenting a hydraulic diameter twice the MSE. The MTB performance index was three times greater than the MSE performance index for the same operating conditions.

The MTB W3000H400 was employed as a millireactor in the biodiesel synthesis, presenting a maximum conversion of 92.67%

Appendix A. Mathematical modeling and numerical details

The fluid dynamic and chemical reaction studies were accomplished using the computational code ANSYS CFX 17.0. It is based on the solution of conservation equations of transport properties, using an Element-Based Finite Volume Method in the numerical procedure. In this research, the conservation of total mass (continuity) (Eq. A.1), momentum (Navier-Stokes) (Eq. A.2) and mass of chemical species (Eq. A.3) were solved for incompressible, steady-state and laminar flow conditions:

$$\nabla \cdot U = 0 \quad (\text{A.1})$$

$$\rho (U \cdot \nabla U) = -\nabla p + \mu \nabla^2 U + \rho g \quad (\text{A.2})$$

$$\rho (U \cdot \nabla Y_i) = \rho D_i \nabla^2 Y_i + S_i \quad (\text{A.3})$$

where ρ is the specific mass (kg m^{-3}), U is the velocity vector (m s^{-1}), μ is the dynamic viscosity (Pa s), g is the gravity acceleration (m s^{-2}), p is the pressure ($\text{kg m}^{-1} \text{s}^{-2}$), Y is the mass fraction, D_i is the kinematic diffusion coefficient ($\text{m}^2 \text{s}^{-1}$) and S is the mass source due to chemical reactions ($\text{kg m}^{-3} \text{s}^{-1}$), modeled in accordance with Eq. A.4:

$$S_i = \left(\sum_{r_r}^n \nu_i^{''} r_r - \sum_{r_r}^n \nu_i' r_r \right) M_{W_i} \quad (\text{A.4})$$

where M_W is the molecular weight, $\nu^{''}$ e ν' are the stoichiometric coefficient of species as products or as reactants, respectively, at chemical reaction r and r_r is the rate of reaction r .

The mass diffusion coefficient of ethanol ($1.2 \times 10^{-9} \text{ m}^2 \text{s}^{-1}$) was estimated using the Wilke-Chang correlation [45], considering ethanol in sunflower oil. For the other species, the mass diffusivity coefficients were estimated on their viscosities using the ethanol-oil diffusion coefficient as reference [46].

For all cases, a multicomponent flow was considered under isothermal, incompressible and laminar flow regime conditions. The chemical reactions were considered to be in equilibrium state. For the numerical solution, high order discretization schemes were employed. A convergence criteria of $\text{RMS} = 1 \times 10^{-6}$ was defined for a solving iteration range of 500-5000. The simulations were solved in parallel processing using computer nodes with 8 Intel Xeon 3 GHz, 16GB RAM processors using Linux Suse 64-bit OS.

The advection terms of transport equation were interpolated by a high order Upwind scheme. Shape functions were employed to interpolate diffusion and pressure gradient terms [47]. These functions were derived from Finite Element Method, being used to estimate the flow properties

and a residence time of 30 s. The MTB millireactor performance was also compared with other microdevices with the same longitudinal length of 35 mm. The MTB exhibited the superior oil conversion among the presented microreactors, even with the dimensions of a millichannel, standing out the good performance achieved by the proposed design.

For the water/ethanol mixing process, the geometry W1500H200 was employed. High mixing indexes of 0.99 were obtained for low Reynolds number (0.1) and also for the higher Reynolds numbers of 50 and 100. It was demonstrated the capability of the milliscale MTB design to achieve high mixing performance concerning high efficiency microdevices, presenting in some cases, superior performance. At $Re = 0.1$, high mixing efficiency of $M \geq 0.90$ was achieved in only 3.5 mm of channel length. Nevertheless, for higher Reynolds number, at least 10.5 mm were necessary ($Re = 100$).

In future studies, our research group intends to perform experimental runs with the MTB design. The millidevices will be manufactured based on the optimal geometries detailed in the present study. The experimental mixing performance will be carried out by the Villermaux-Dushman method. Moreover, biodiesel synthesis and other chemical synthesis (e.g. pharmaceutical synthesis) will be accomplished.

Acknowledgements

The authors would like to thank the National Postdoctoral Program (PNPD/Capes), the Unicamp Scholarship Program, and the financial support provided by CNPq (National Council for Scientific and Technological Development, Process 404760/2016-3), FAPESP (São Paulo Research Foundation, Process 2016/20842-4) and FAPEMIG (Minas Gerais Research Foundation, Process APQ-02144-17).

values inside the control volume. In general, the Ansys CFX uses a tri-linear shape function based on parametric coordinates. The transport property value, Φ , of a control volume is then given by the summation over all control volumes nodes of the product between the shape function value and the nodal value ($\Phi_{CV} = \sum N_i \Phi_i$, where Φ_{CV} is the control volume transport property, N_i is the shape function value - $N_i = 1$, if $i = j$ and $N_i = 0$ if $i \neq j$ - and Φ_i is the nodal value of transport property. Note that for a tetrahedral control volume, there is four nodes).

The ANSYS CFX employs a coupled solver for the transport equation system, based on Richie and Chow [48] discretization method modified by Majumbar [49], to eliminate the time-step dependence for steady-state simulations. The Algebraic Multigrid Method was used to improve the convergence in linear equation system solution procedure. This method provides a virtual coarsening of mesh spacing during the iteration process, then, a re-refinement is performed in the numerical mesh to acquire an accurate solution [47].

The initial and boundary conditions employed in the numerical solution of transport equations are described below:

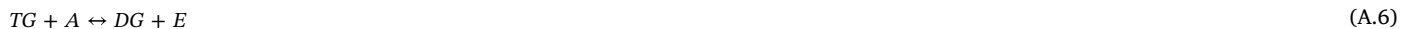
- Alcohol feed stream (Inlet 1): pure alcohol flowing into domain ($Y_A = 1$; $Y_{TG} = 0$ or $Y_W = 0$), with uniform velocity normal to boundary inlet surface ($u = U_A$);
- Sunflower oil feed stream or water feed stream (Inlet 2): pure oil (triglyceride) or water stream flowing into domain ($Y_{TG} = 1$ or $Y_W = 1$; $Y_A = 0$), with uniform velocity normal to boundary inlet surface ($u = U$). Both inlet velocities were defined based on Reynolds number (Eq. A.5) and ethanol/oil molar ratio.
- Microchannel outlet (Outlet): zero relative average pressure;
- Microchannel walls (Walls): no-slip condition at solid surfaces.

$$Re = \frac{ud_H}{\nu} \quad (A.5)$$

where d_H is the hydraulic diameter (m) and ν is the kinematic viscosity ($m^2 s^{-1}$).

Appendix B. Reaction kinetics

Transesterification reaction can be described by a series of three consecutive reversible reaction steps, according to Eqs. A.6–A.8. In general, the tri- (TG), di- (DG) and mono- (MG) glycerides combine with an alcohol molecule (A) in alkaline medium at each step, producing an ethyl ester (E) molecule, until it finally produces the glycerol (GL) (Freedman et al. [50]):



The overall biodiesel synthesis reaction expression is given by Eq. A.9:



Marjanovic et al. [51] proposed an expression for the triglyceride reaction rate at equilibrium state, according to Eq. A.10:

$$-r_{TG} = -\frac{dC_{TG}}{dt} = \vec{k}_{TG} C_A - \overleftarrow{k}_{TG} C_{GL} C_E \quad (A.10)$$

where $-r$ is the reaction rate ($mol m^{-3} s^{-1}$), \vec{k} and \overleftarrow{k} are the reaction rate constants for direct and reverse reactions ($m^3 mol^{-1} s^{-1}$), respectively, C is the molar concentration ($mol m^{-3}$), and the subscripts TG, A, GL and E denote triglyceride, alcohol, glycerol and ethyl ester species. The kinetic data employed in simulations are given in Table A1.

The mass conservation of species present in the system, based on the overall chemical reaction (Eq. A.9) is described by Eqs. (A.11)–(A.14):

$$\rho(U \cdot \nabla Y_{TG}) = \rho D_{TG} \nabla^2 Y_{TG} + (r_{TG}) M_{WTG} \quad (A.11)$$

$$\rho(U \cdot \nabla Y_A) = \rho D_A \nabla^2 Y_A + (3r_{TG}) M_{WA} \quad (A.12)$$

$$\rho(U \cdot \nabla Y_{GL}) = \rho D_{GL} \nabla^2 Y_{GL} + (-r_{TG}) M_{WGL} \quad (A.13)$$

$$\rho(U \cdot \nabla Y_E) = \rho D_E \nabla^2 Y_E + (-3r_{TG}) M_{WE} \quad (A.14)$$

For the reactive system, inert oil (with similar physical properties of sunflower oil) was added in system as a constraint, in order to ensure the mass fraction restriction (Eq. A.15):

$$\sum_i^n Y_i = 1 \quad \therefore \quad Y_{INERT\ OIL} = 1 - Y_{TG} - Y_A - Y_{GL} - Y_E \quad (A.15)$$

Table A1

Kinetic data employed in the numerical simulations.

Temperature (°C)	Ethanol/oil molar ratio	NaOH concentration (wt. %)	$\vec{k} \times 10^6$ ($m^3 mol^{-1} s^{-1}$)	$\overleftarrow{k} \times 10^8$ ($m^3 mol^{-1} s^{-1}$)
50	9:1	1.00	15.68	9.42

References

- [1] C. Ramshaw, The incentive for process intensification, Proceedings, 1st Int'l. Conf. Proc. Intensif. for Chem. Ind. 18 (1995) 1.
- [2] R.C. Lo, Application of microfluidics in chemical engineering, *Chem. Eng. Process Tech.* 1 (2013) 1002.
- [3] H.S. Fogler, Elements of Chemical Reaction Engineering, fourth ed., Upper Saddle River, NJ, Prentice Hall PTR, 2006.
- [4] G.M. Whitesides, The origins and the future of microfluidics, *Nature* 442 (2006) 368–373.
- [5] A. Skardal, S.V. Murphy, M. Devarasetty, I. Mead, H.-W. Kang, Y.-J. Seol, Y.S. Zhang, S.-R. Shin, L. Zhao, J. Aleman, A.R. Hall, T.D. Shupe, A. Kleensang, M.R. Dokmei, S.J. Lee, J.D. Jackson, J.J. Yoo, T. Hartung, A. Khademhosseini, S. Soker, C.E. Bishop, A. Atala, Multi-tissue interactions in an integrated three-tissue organ-on-a-chip platform, *Sci. Rep.* 7 (2017) 8837.
- [6] S. Cardoso, D.C. Leitao, T.M. Dias, J. Valadeiro, M.D. Silva, A. Chicharo, V. Silveiro, J. Gaspar, P.P. Freitas, Challenges and trends in magnetic sensor integration with microfluidics for biomedical applications, *J. Phys. D Appl. Phys.* 50 (2017).
- [7] H.S. Santana, D.S. Tortola, J.L. Silva Jr., O.P. Taranto, Biodiesel synthesis in micromixer with static elements, *Energy Convers. Manage.* 141 (2017) 28–39.
- [8] H.S. Santana, D.S.G.B. Sanchez, O.P. Taranto, Evaporation of excess alcohol in biodiesel in a microchannel heat exchanger with Peltier module, *Chem. Eng. Res. Des.* 124 (2017) 20–28.
- [9] J. Zhang, K. Wang, Teixeira A.R, K.F. Jensen, G. Luo, Design and scaling up of microchemical systems: a review, *Annu. Rev. Chem. Biomol. Eng.* 8 (2017) 285–305.
- [10] J. Melo, Usinas de Biodiesel em Pernambuco. <https://www.biodieselbr.com/noticias/columnistas/convidado/usinas-biodiesel-pernambuco-300410.htm>, 2017 (accessed 16 november 2017).
- [11] G. Guan, M. Teshima, C. Sato, S.M. Son, M.F. Irfan, K. Kusakabe, Two-phase behavior in microtube reactors during biodiesel production from waste cooking oil, *Env. Energy Eng.* 56 (2010) 1383–1390.
- [12] J. Sun, J. Ju, L. Zhang, N. Xu, Synthesis of biodiesel in capillary microreactors, *Ind. Eng. Chem. Res.* 47 (2008) 1398–1403.
- [13] K.D. Nagy, B. Shen, T.F. Jamison, K.F. Jensen, Mixing and dispersion in small-scale flow systems, *Org. Process Res. Dev.* 16 (2012) 976–981.
- [14] N. Solehati, J. Bae, A.P. Sasmito, Numerical investigation of mixing performance in microchannel T-junction with wavy structure, *Comput. Fluids* 96 (2014) 10–14.
- [15] M.A. Sultan, C.P. Fonte, M.M. Dias, J.C.B. Lopes, R.J. Santos, Experimental study of flow regime and mixing in T-jets mixers, *Chem. Eng. Sci.* 73 (2012) 388–399.
- [16] C.-Y. Lee, L.-M. Fu, Recent advances and applications of micromixers, *Sens. Actuators B Chem.* 259 (2018) 677–702.
- [17] W. Ruijin, L. Beiqi, S. Dongdong, Z. Zefei, Investigation on the splitting-merging passive micromixer based on Baker's transformation, *Sens. Actuators B Chem.* 249 (2017) 395–404.
- [18] N.-T. NGUYEN, Z. WU, Micromixers – a review, *J. Micromech. Microeng.* 15 (2005) 1–16.
- [19] N.-T. NGUYEN, Micromixers, Fundamentals, Design and Fabrication, second ed., William Andrew, 2012.
- [20] X. Chen, T. Li, A novel passive micromixer designed by applying an optimization algorithm to the zigzag microchannel, *Chem. Eng. J.* 313 (2017) 1406–1414.
- [21] H.S. Santana, J.L. Silva Jr., O.P. Taranto, Numerical simulations of biodiesel synthesis in microchannels with circular obstructions, *Chem. Eng. Process.* 98 (2015) 137–146.
- [22] H. Bockelmann, D.P.J. Barz, Optimised active flow control for micromixers and other fluid applications: sensitivity- vs. Adjoint-based strategies, *Comput. Fluids* 106 (2015) 93–107.
- [23] N. Veldurthi, S. Chandel, T. Bhave, D. Bodas, Computational fluid dynamic analysis of poly(dimethylsiloxane) magnetic actuator based micromixer, *Sens. Actuators B Chem.* 212 (2015) 419–424.
- [24] Y. Su, A. Lautenschleger, G. Chen, E.Y. Kenig, A numerical study on liquid mixing in multichannel micromixers, *Ind. Eng. Chem. Res.* 53 (2014) 390–401.
- [25] N. Tran-Minh, T. DONG, F. Karlsen, An efficient passive planar micromixer with ellipse-like micropillars for continuous mixing of human blood, *Comput. Methods Programs Biomed.* 117 (2014) 20–29.
- [26] G. Xia, J. Li, X. Tian, M. Zhou, Analysis of flow and mixing characteristics of planar asymmetric split-and-Recombine (P-SAR) micromixers with fan-shaped cavities, *Ind. Eng. Chem. Res.* 51 (2012) 7816–7827.
- [27] M.S. Cheri, H. Latifi, M.S. Moghaddam, H. Shahroki, Simulation and experimental investigation of planar micromixers with short-mixing-length, *Chem. Eng. J.* 234 (2013) 247–255.
- [28] A. Afzal, Kim K-Y, Passive split and recombination micromixer with convergent-divergent walls, *Chem. Eng. J.* 203 (2012) 182–192.
- [29] A. Alam, A. Afzal, K.-Y. Kim, Mixing performance of a planar micromixer with circular obstructions in a curved microchannel, *Chem. Eng. Res. Des.* 92 (2014) 423–434.
- [30] R. Kamali, A. Mansoorifar, M.K. Dehghan Manshadi, Effect of baffle geometry on mixing performance in the passive micromixers, *IJST* 38 (M2) (2014) 351–360.
- [31] C.K. Chung, T.R. Shih, C.K. Chang, C.W. Lai, B.H. Wu, Design and experiments of a short-mixing-length baffled microreactor and its application to microfluidic synthesis of nanoparticles, *Chem. Eng. J.* 168 (2011) 790–798.
- [32] H.S. Santana, D.S. Tortola, J.L. Silva Jr., O.P. Taranto, Transesterification reaction of sunflower oil and ethanol for biodiesel synthesis in microchannel reactor: experimental and simulation studies, *Chem. Eng. J.* 302 (2016) 752–762.
- [33] H.S. Santana, D.S. Tortola, J.L. Silva Jr., O.P. Taranto, Transesterification of sunflower oil in microchannels with circular obstructions, *Chin. J. Chem. Eng.* 26 (2017) 852–863.
- [34] S. Schwarz, E.S. Borovinskaya, W. Reschetilowski, Base catalyzed ethanolation of soybean oil in microreactors: experiments and kinetic modeling, *Chem. Eng. Sci.* 104 (2013) 610–618.
- [35] P. Sun, B. Wang, J.Z.L. Yao, N. Xu, Fast synthesis of biodiesel at high throughput in microstructured reactors, *Ind. Eng. Chem. Res.* 49 (2010) 1259–1264.
- [36] E. Santacesaria, M. Di Serio, R. Tesser, R. Turco, M. Tortorelli, V. Russo, Biodiesel process intensification in a very simple microchannel device, *Chem. Eng. Process.* 52 (2012) 47–54.
- [37] M. Rahimi, B. Aghel, M. Alitabar, A. Sepahvand, H.R. Ghasempour, Optimization of biodiesel production from soybean oil in a microreactor, *Energy Convers. Manag.* 79 (2014) 599–605.
- [38] C.K. Chung, T.R. Shih, A rhombic micromixer with asymmetrical flow for enhancing mixing, *J. Micromech. Microeng.* 17 (2007) 2495–2504.
- [39] M.A. Ansari, K.-Y. Kim, Mixing performance of unbalanced split and recombine micromixers with circular and rhombic sub-channels, *Chem. Eng. J.* 162 (2010) 760–767.
- [40] T. Xie, C. Xu, Numerical and experimental investigations of chaotic mixing behavior in a oscillating feedback micromixer, *Chem. Eng. Sci.* 171 (2017) 303–317.
- [41] X. Chen, J. Shen, Numerical and experimental investigation on splitting-and-recombination micromixer with E-shape mixing units, *Microsyst. Technol.* 23 (2017) 4671–4677.
- [42] X. Chen, Z. Zhang, D.Y.Z. Hu, Numerical studies on different two-dimensional micromixers basing on a fractal-like tree network, *Microsyst. Technol.* 23 (2017) 755–763.
- [43] J. Clark, M. Kaufman, P.S. Fodor, Mixing enhancement in serpentine micromixer with a non-rectangular cross-section, *Micromachines* 9 (2018).
- [44] S. Hossain, M.A. Ansari, A. Husain, K.-Y. Kim, Analysis and optimization of a micromixer with a modified Tesla structure, *Chem. Eng. J.* 158 (2010) 305–314.
- [45] R.B. Bird, W.E. Stewart, E.N. Lightfoot, *Transport Phenomena*, John Wiley & Sons, United State of America, 2002.
- [46] Ansys Inc.. ANSYS CFX-Solver Theory Guide. 2009.
- [47] Ansys Inc., ANSYS CFX-Pre User's Guide Release 14.0; 2011.
- [48] C.M. Rhee, W.L. Chow, A numerical study of the turbulent flow past an isolated airfoil with trailing edge separation, *AIAA Paper* 82 (1982) 0998.
- [49] S. Majumdar, Role of underrelaxation in momentum interpolation for calculation of flow with nonstaggered grids, *Numeric Heat Transfer.* 13 (1988) 125–132.
- [50] B. Freedman, E.H. Pryde, T.L. Mounts, Variables affecting the yields of fatty esters from transesterified vegetable oils, *J. Am. Oil Che. Soc* 61 (1984) 138–1643.
- [51] A.V. Marjanovic, O.S. Stamenkovic, Z.B. Todorovic, M.L. Lazic, V.B. Veljkovic, Kinetics of the base-catalyzed sunflower oil ethanolation, *Fuel* 89 (2010) 665–671.

Harrison Silva Santana, PhD earned his PhD in Chemical Engineering from University of Campinas, Brazil in 2016. His PhD thesis was the investigation of biodiesel synthesis in microchannels. In 2015 he spent several months in the group of Prof. Lee Cronin at the University of Glasgow (UK) studying the application of microwaves in inorganic reactions and manufacture of microdevices using 3D printers. He is currently an associate researcher working in the field of microchemical plants and the use of 3D printers in chemical processes. He has published several articles exploring from numerical simulations in the development of microdevices to the use of Microfluidics in chemical reactions and unit operations. His scientific interest focuses on transport phenomena in microfluidic systems and 3D printers applied to chemical processes in microscale.

João Lameu Silva Jr., Professor. Chemical Engineer graduated in 2009, is currently Professor at the Federal Institute Education, Science and Technology of the South of Minas, Campus Pouso Alegre and collaborator in research projects in the area of Microfluidics. Master and PhD degrees by the School of Chemical Engineering at the University of Campinas (FEQ/UNICAMP). He performed researches in UNICAMP/Petrobras Cooperation projects in the Laboratory of Chemical Processes and Corporate Management (PQGe), Department of Process Engineering of the School of Chemical Engineering/UNICAMP, between 2010 and 2015. He has experience in the area of Transport Phenomena and Particulate Systems, Microfluidics and Numerical Simulation using Computational Fluid Dynamics (CFD).

Osvaldir Pereira Taranto, Professor. He is currently a Full Professor at the University of Campinas. Has experience in Chemical Engineering, acting on the following subjects: drying, jetting bed, fluidized bed, coating and fluid dynamics.